

Prognostic Modeling Studies of the Keweenaw Current in Lake Superior. Part II: Simulation

JIANRONG ZHU,* CHANGSHENG CHEN,⁺ ELISE RALPH,[#] SARAH A. GREEN,[@]
JUDITH WELLS BUDD,[&] AND FRANK Y. ZHANG**

* *State Key Laboratory for Estuarine and Coastal Research, East China Normal University,
Shanghai, China*

⁺ *Department of Marine Sciences, University of Georgia, Athens, Georgia*

[#] *Great Lakes Observatory, University of Minnesota, Duluth, Minnesota*

[@] *Department of Chemistry, Michigan Technological University, Houghton, Michigan*

[&] *Department of Geological Engineering and Sciences, Michigan Technological University,
Houghton, Michigan*

** *Department of Biology, Kean University, Union, New Jersey*

(Manuscript received 5 February 1999, in final form 15 March 2000)

ABSTRACT

The Keweenaw Current, observed along the coast of the Keweenaw Peninsula in Lake Superior during July 1973, was simulated using a 3D, nonorthogonal coordinate transformation, primitive equation coastal ocean model. The model domain covered the entire lake with a high resolution of 250–600 m in the cross-shelf direction and 4–6 km in the alongshelf direction along the peninsula. The model was initialized using the monthly averaged temperature field observed in June 1973 and was run prognostically with synoptic wind forcing plus monthly averaged heat flux. Good agreement was found between model-predicted and observed currents at buoy stations near Eagle Harbor. Comparison of the model results with and without inclusion of heat flux suggested that combined wind and heat fluxes played a key role in the intensification of the Keweenaw Current during summer months. The model-predicted relatively strong near-inertial oscillations occurred episodically under conditions of a clockwise-rotating wind. These oscillations intensified at the surface, were weak near the coast, and increased significantly offshore.

1. Introduction

Along the western shore of Lake Superior's Keweenaw Peninsula (Fig. 1), the coastal current is characterized by a strong alongshelf jet known as the Keweenaw Current (Harrington 1895). The occurrence and evolution of this jet are closely related to the thermal front (or thermal bar) that forms in early summer as stratification develops and intensifies due to surface heating and wind mixing (Bennett 1978). Based on hydrographic and current measurements, which were taken across the shelf and at current moorings off Eagle Harbor in 1973, the Keweenaw Current is closely linked to the temporal variation of the thermal front and winds (Niebauer et al. 1977). The current was located over a sharp slope near the coast, with a cross-shelf scale of less than 10 km (Fig. 2). It weakened remarkably as the thermal front was advected offshore during the period

of upwelling-favorable wind (Fig. 2a) and intensified significantly as the thermal front was advected onshore during the period of downwelling-favorable wind (Fig. 2b). The maximum speed of this current reached about 50–65 cm s⁻¹ during the northeastward wind period.

The physical processes that control the formation, evolution, and perturbation of the Keweenaw Current and thermal front in Lake Superior have not been fully explored. Niebauer et al.'s (1977) studies have provided a comprehensive view of the Keweenaw Current and its relation to the temporal variation of the thermal front during coastal downwelling and upwelling cycles, but physical processes involving the interaction between buoyancy and wind-driven flows have not been quantified. Was the current driven dominantly by wind only? Did the surface heating play a role in the intensification of the jet during summer? Are physical processes controlling the amplitude of the jet the same in downwelling and upwelling cycles? To our knowledge, these questions have not been fully addressed.

To date, no modeling efforts have been successful in simulating the Keweenaw Current. Previous modeling

Corresponding author address: Dr. Changsheng Chen, Department of Marine Sciences, University of Georgia, Athens, GA 30602.
E-mail: chen@whale.marsci.uga.edu

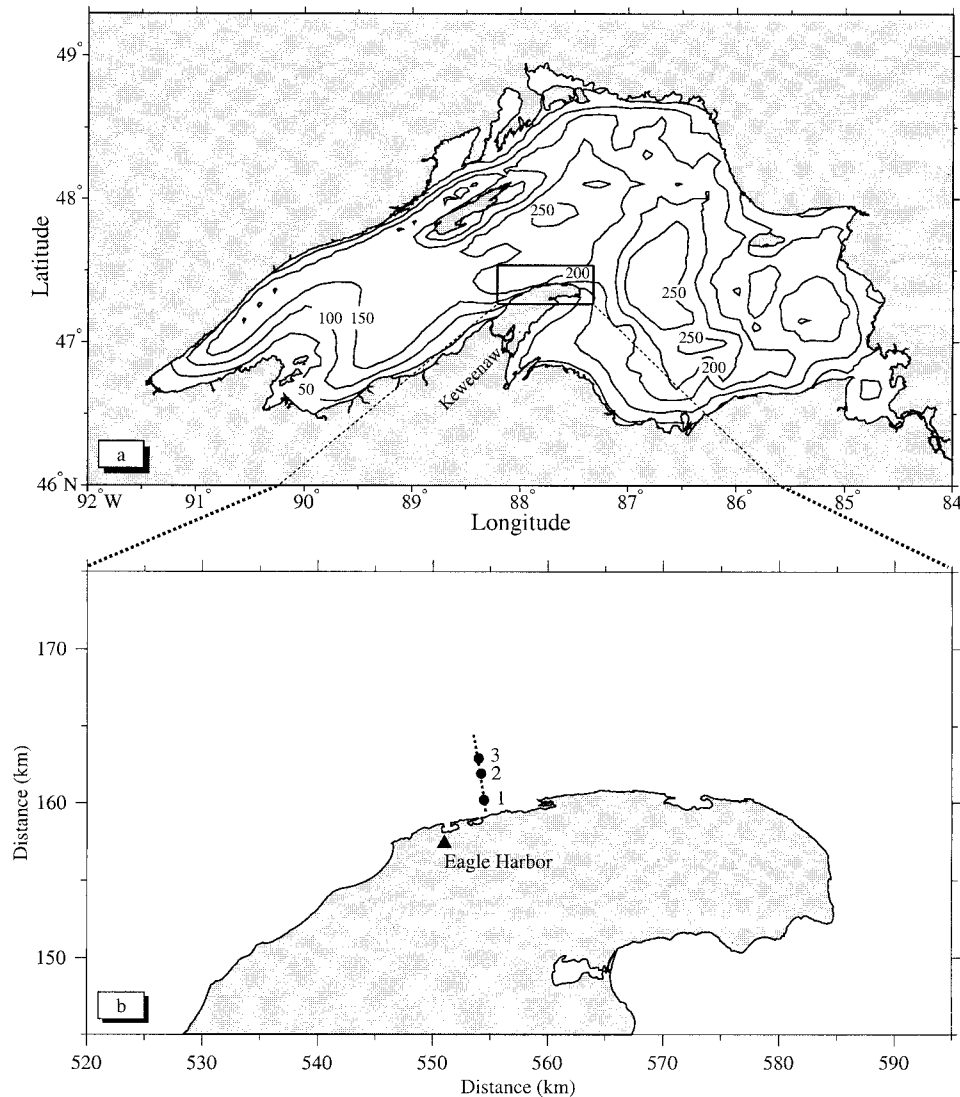


FIG. 1. Bottom topography (in meters) of (a) Lake Superior and (b) moored buoy sites. Solid circles are the locations of moored current meters labeled 1–3, and the dashed line is the section used to present the cross-shelf distribution of currents and temperature in the paper.

explorations of this current were based mainly on layered models for either idealized or realistic wind forcing (Diehl et al. 1977; Lam 1978). A four-layer model forced by realistic wind and buoyancy forcings, which was used by Lam (1978), did produce a current jet along the Keweenaw coast, but the model-predicted speed was only about $5\text{--}7\text{ cm s}^{-1}$, that is, 5–10 times smaller than that observed by Niebauer et al. (1977). This underestimation of the speed likely had two causes: 1) the low cross-shelf model resolution and 2) the lack of surface heating. A uniform horizontal resolution of 10 km was used in Lam's (1978) model experiment, which was larger than the general cross-shelf scale of the Keweenaw Current observed in summer. Therefore, it was not surprising that his model failed to predict the proper

magnitude of the current. Heating should play an important role in maintaining the thermal front during the summer (Schertzer 1978). Since the Keweenaw Current is driven by both buoyancy (thermal front) and wind forcing, the lack of surface heating may cause underestimates of the thermal front's intensity and the jet magnitude.

Simulating the Keweenaw Current requires a model with high resolution in the cross-shelf direction. Since this current usually stays very close to the coast, a proper fitting of the coastline is needed to resolve well the cross-shelf structure of this motion. For this reason, a nonorthogonal coordinate transformation model has been developed for Lake Superior (Chen et al. 2000, manuscript submitted to *J. Atmos. Oceanic Technol.*).

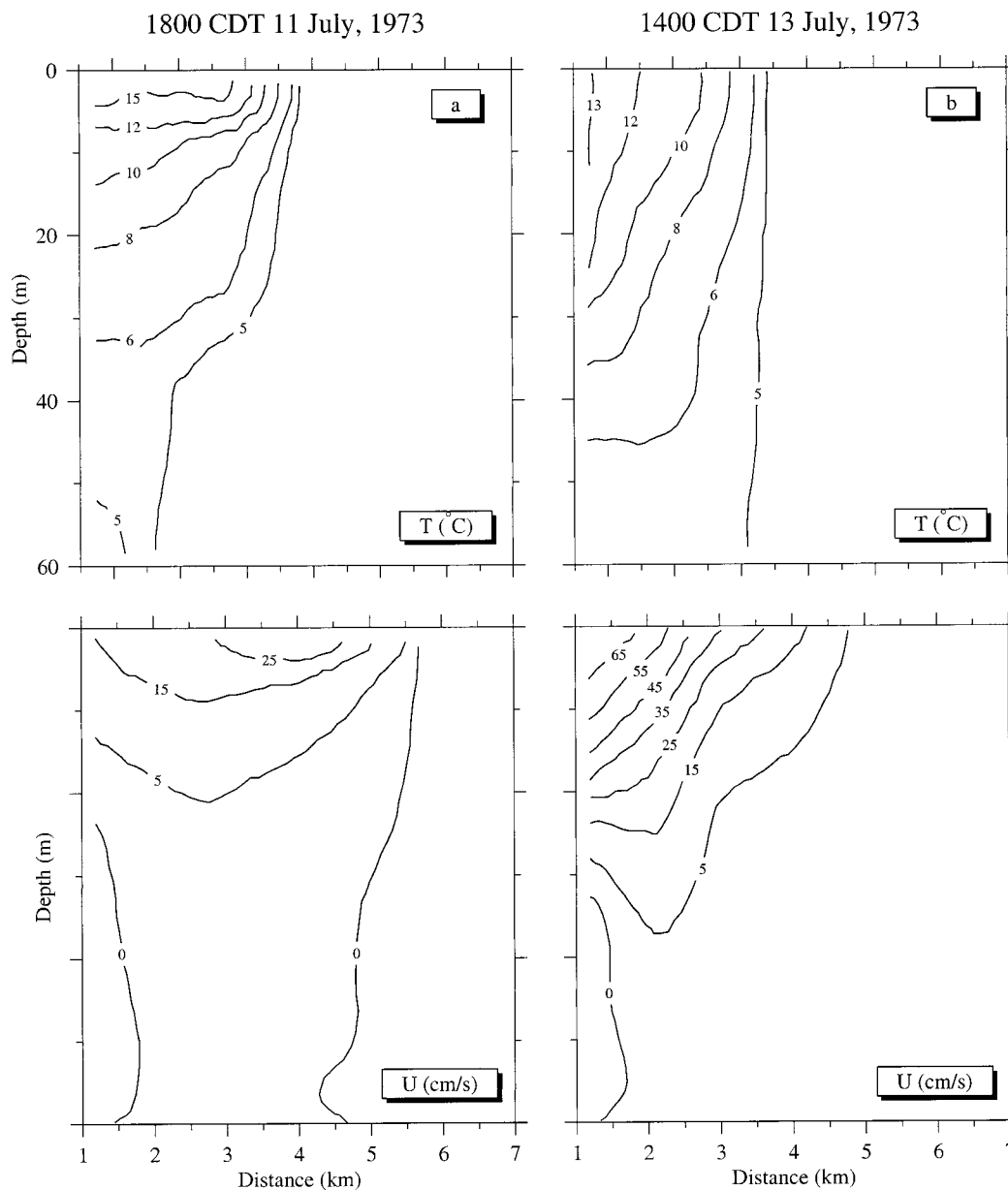


FIG. 2. Cross-shelf distributions of observed temperature and along-shelf baroclinic geostrophic current relative to the bottom at 11 and 13 July 1973. The data used for the plot were directly digitized from Figs. 8 and 9 in Niebauer et al. (1977).

Process studies conducted in Part I (Chen et al. 2001) have provided a view of the dynamics of the thermal front and its relation to the Keweenaw Current. As a continuation of this work, the Keweenaw Current as observed in July 1973 has been simulated by using the observed atmospheric forcing.

The remaining sections are organized as follows. The physical model and numerical designs are described in section 2. The model results of the simulation are presented in section 3, and the physical processes that control the magnitude of the jet are examined in section 4. Finally, a summary is given in section 5.

2. Numerical model and experiment design

The numerical model used in this study is a 3D, non-orthogonal coordinate transformation, coastal ocean circulation model developed by Chen et al. (2000, submitted to *J. Atmos. Oceanic Technol.*). This model is a modified version of the Blumberg and Mellor (1987) 3D primitive equation model with new nonorthogonal coordinates. The model incorporated a free surface for wave simulation and the Mellor and Yamada (1982) level-2.5 turbulent-closure scheme for parameterization of vertical mixing. The model configuration for Lake

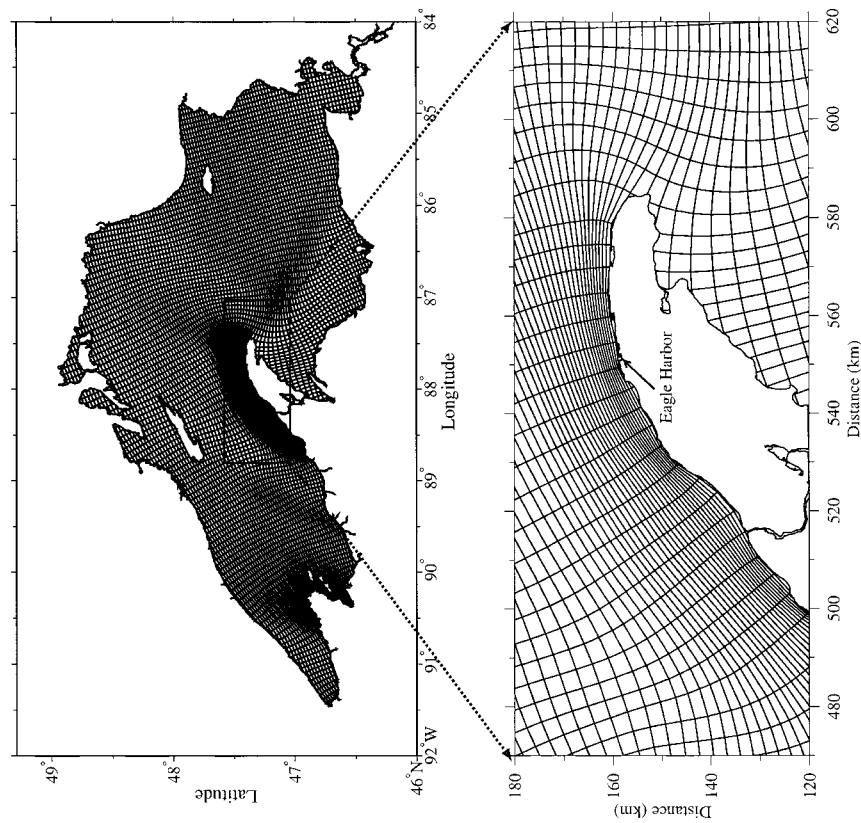


FIG. 3. Numerical grids of the Lake Superior model. The grids were almost orthogonal inside the lake except along the Keweenaw coast where nonorthogonal quadrilaterals were used to fit the shape of the coastline. The horizontal resolution is about 250–600 m in the cross-shelf direction and about 4–6 km in the along-shelf direction along the Keweenaw Peninsula.

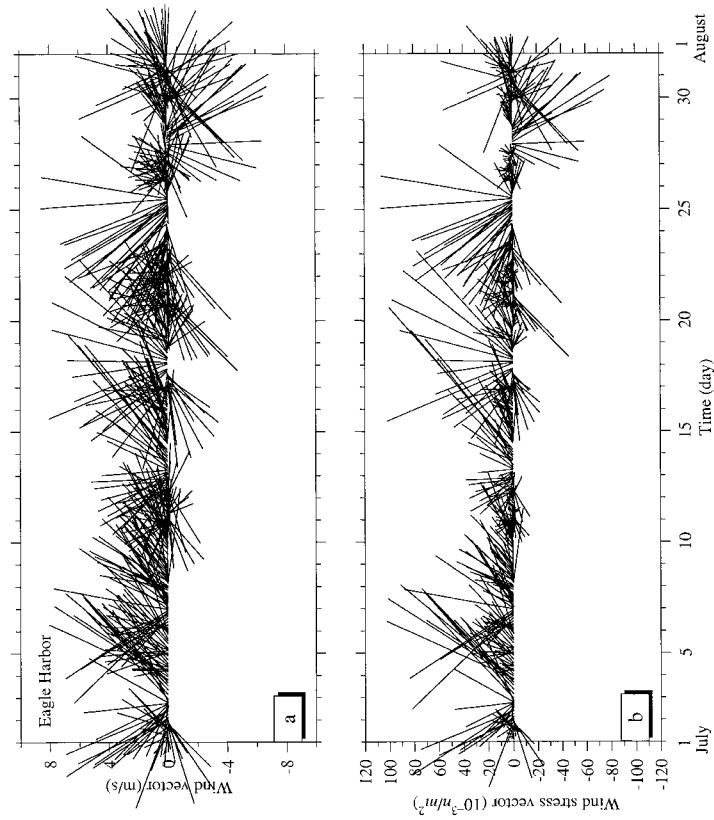


FIG. 4. Time series (a) of observed wind and (b) calculated wind stress vectors at Eagle Harbor for July 1973. The wind data were digitized from Fig. 3 in Niebauer et al. (1977).

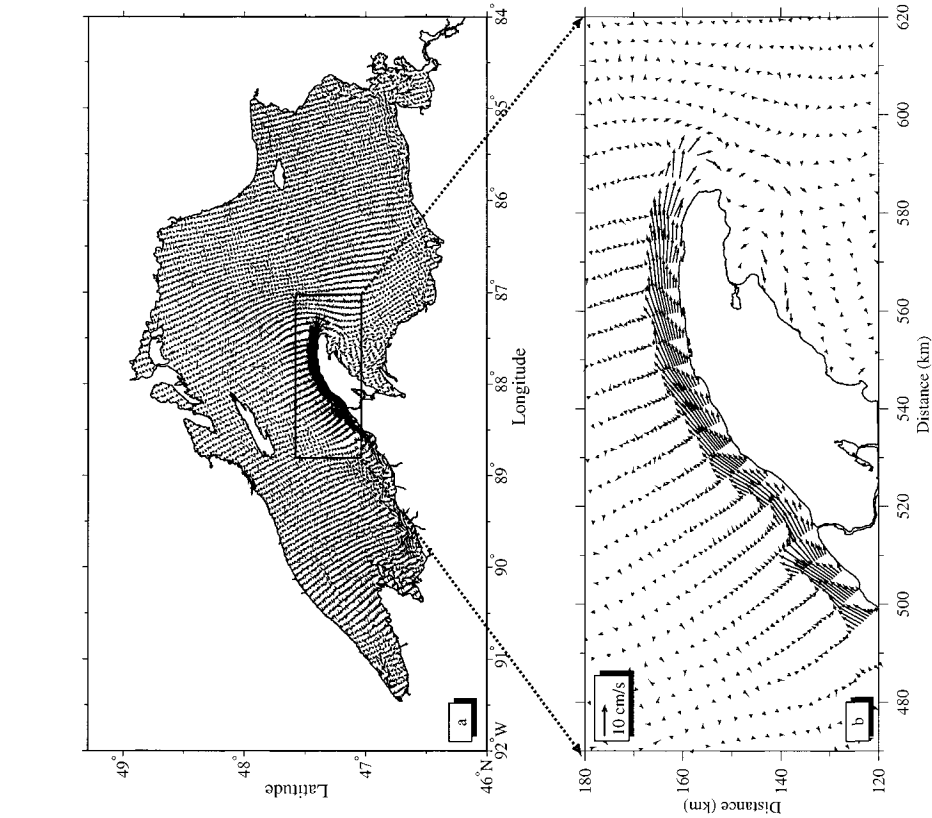


FIG. 5. Distributions of initial temperature at (a) the surface and (b) on the cross-lake section. Dashed line in the upper panel indicates the location of the section used in the lower panel. The contour interval for temperature is 1°C.

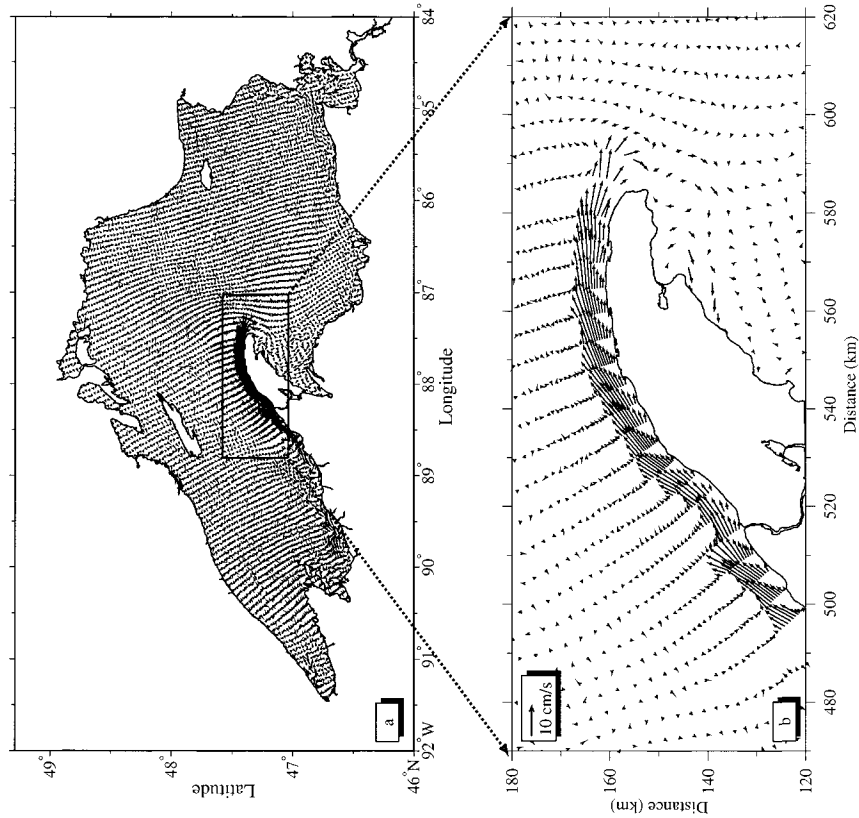


FIG. 6. Map of surface currents at the end of the first model day after the Rossby adjustment of the current field to the density field. The current vector scale is given in the upper-left corner in panel b.

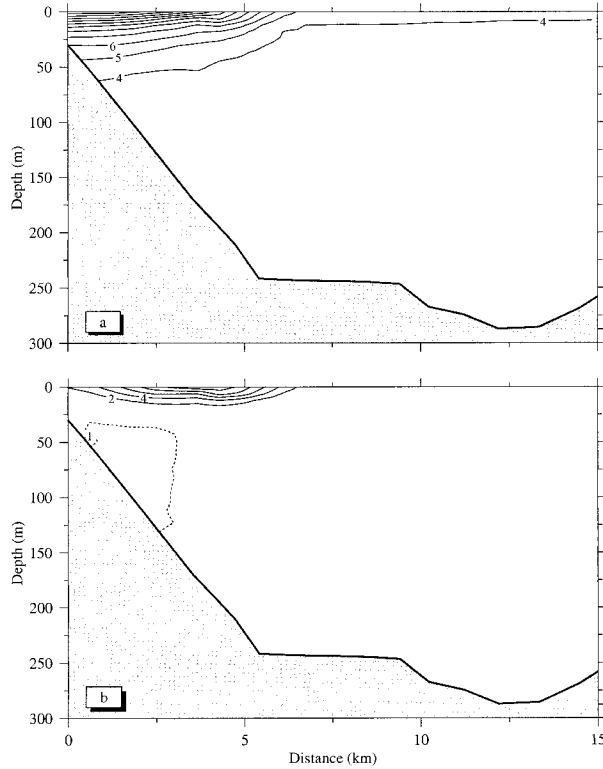


FIG. 7. Cross-shelf distributions of (a) temperature, (b) along-shelf current, and (c) cross-shelf current at the end of the first model day after the Rossby adjustment of current filed to density field.

Superior was given in Part I of these modeling experiments.

The model domain covered the entire volume of the lake (Fig. 3), with higher resolution near the Keweenaw coast. The model grids were almost orthogonal in the interior of the lake except along the Keweenaw coast where nonorthogonal quadrilaterals were used to fit the shape of the coastline. The horizontal resolution was about 250–600 m in the cross-shelf direction and about 4–6 km in the alongshelf direction along the Keweenaw Peninsula. A σ -coordinate transformation (31 levels) was used in the vertical, which corresponds to a vertical resolution of about 1 m near the coast and 8.3 m at the 250-m isobath offshore. The time step of the numerical integration was 360 s.

The model was forced by the wind stress and monthly averaged heat flux calculated from observations acquired in July 1973 near Eagle Harbor and was run over the entire month of July. The surface wind stress (Fig. 4) was calculated using Large and Pond's (1980) formula with a neutral, steady-state drag coefficient. The heat forcing included two parts: 1) the surface net heat flux, and 2) the downward shortwave irradiance. The absorption of downward irradiance was assumed to be an exponential function of depth given by

$$I(z, t) = \frac{I_o(t)}{\rho c_p} [R e^{z/\xi_1} + (1 - R) e^{z/\xi_2}], \quad (1)$$

where $I_o(t)$ is the incident irradiance at the sea surface, ξ_1 and ξ_2 are attenuation lengths, and R is an empirical constant representing the percent of the irradiance received in layers of ξ_1 and ξ_2 thickness. This irradiance form was suggested first by Kraus (1972) and then by Simpson and Dickey (1981a,b). The heat forcing in this case was expressed as a body force in the temperature equation with a form of

$$\hat{H}(z, t) = \frac{\partial I(z, t)}{\partial z} = \frac{I_o(t)}{\rho c_p} \left[\frac{R}{\xi_1} e^{z/\xi_1} + \frac{1 - R}{\xi_2} e^{z/\xi_2} \right]. \quad (2)$$

The surface boundary condition for temperature was given by

$$\left. \frac{\partial T}{\partial z} \right|_{z=\zeta} = \frac{1}{\rho c_p K_h} [Q_n(t) - I_o(t)], \quad (3)$$

where T is temperature, z the vertical coordinate (positive upward), ζ the surface elevation, ρ the mean water density, c_p the specific heat of seawater, K_h the thermal diffusion at the surface, and $Q_n(t)$ is the net surface heat flux. There were no direct measurements of the surface heat flux available in 1973. A monthly averaged estimation of the heat budget in Lake Superior for 1973 was made by Schertzer (1978) with an empirical method. According to this computation, the monthly averaged Q_n and I_o for July 1973 were 484 and 500 cal cm⁻² day⁻¹, respectively, and these values were used in the numerical experiments. Here ξ_1 , ξ_2 , and R were set up using parameters for stratified conditions suggested by Simpson and Dickey (1981a,b): they were 0.35, 23, and 0.58, respectively.

The initial distribution of temperature (Fig. 5) was specified using observed temperature data taken regionally over the lake in late June and calibrated using the high-resolution hydrographic data taken in early July by Niebauer et al. (1973). Surface temperature was about 14°C at the coast and decreased to 5°C over a cross-shelf distance of 5 km. The large horizontal and vertical temperature gradient only existed in the upper 60 m. The model was spun up in two steps. At first, the model ran with only forcing from the initial temperature field for one day. Then, wind (increasing linearly from zero magnitude) was added on the second day to adjust the model-predicted current to the observed current on 1 July 1973. The model was forced with the observed wind beginning at the end of the second model day and continuing for a month simulation. To examine the roles of heat forcing in the maintenance of the thermal bar near the Keweenaw coast, the model was also run for a case without heat flux.

3. Model results

a. Model simulation

The model originally was run as a Rossby adjustment problem with an initial temperature field. The timescale

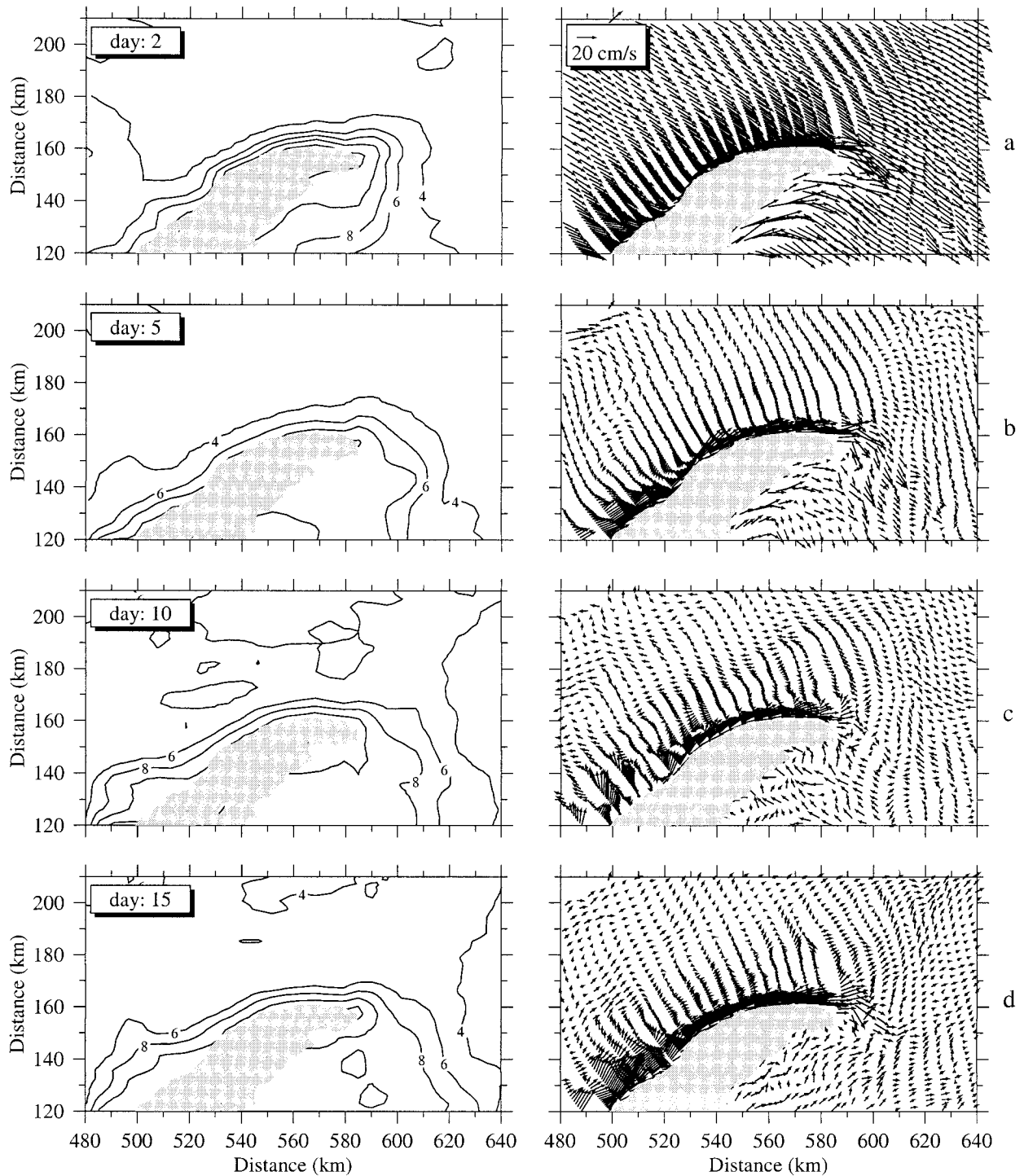


FIG. 8. Surface maps of temperature and current vectors at days 2, 5, 10, and 15. The temperature contour interval is 2°C and the current vector scale is indicated in the upper-left corner in the right of panel a.

of the adjustment of the current to the density field was the local inertial period of approximately 16.4 h. After one model day, a well-defined alongshelf coastal jet formed along the Keweenaw coast due to the large cross-shelf temperature gradient (Fig. 6). The cross-

shelf scale of the jet was about 5 km, with a maximum baroclinic current of 10 cm s^{-1} occurring at a location where the cross-shelf temperature gradient was largest (Fig. 7a). The vertical scale of this current was about 25 m, with a maximum speed at the surface and the

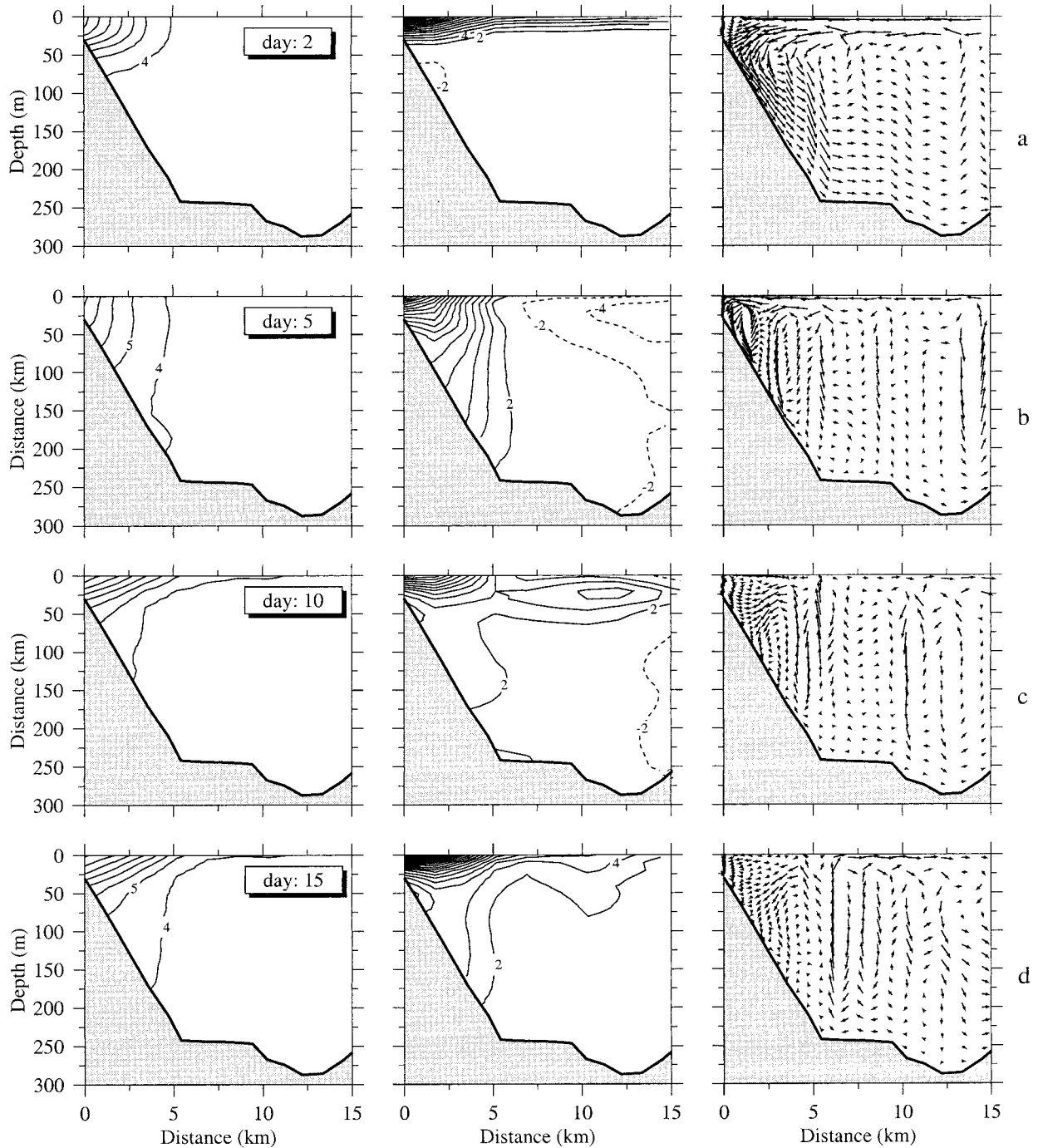


FIG. 9. Cross-shelf sections of (left) temperature, (center) alongshelf current, and (right) cross-shelf current vector at days 2, 5, 10, and 15. The vertical velocity was scaled by a factor of 10^3 in vector plots.

current speed decreases rapidly with depth (Fig. 7b). A weak reversed current of about 1 cm s^{-1} occurred below 25 m along the slope, which was thought to be a result of the baroclinic response of current to the density field. The cross-shelf secondary circulation was characterized by a double-cell circulation with a convergence at the

front near the surface and a divergence in the deep region (Fig. 7c).

The structures of the thermal front and coastal jet current varied significantly with wind. The eastward alongshelf current tended to accelerate dramatically during northward or northeastward winds and to decrease

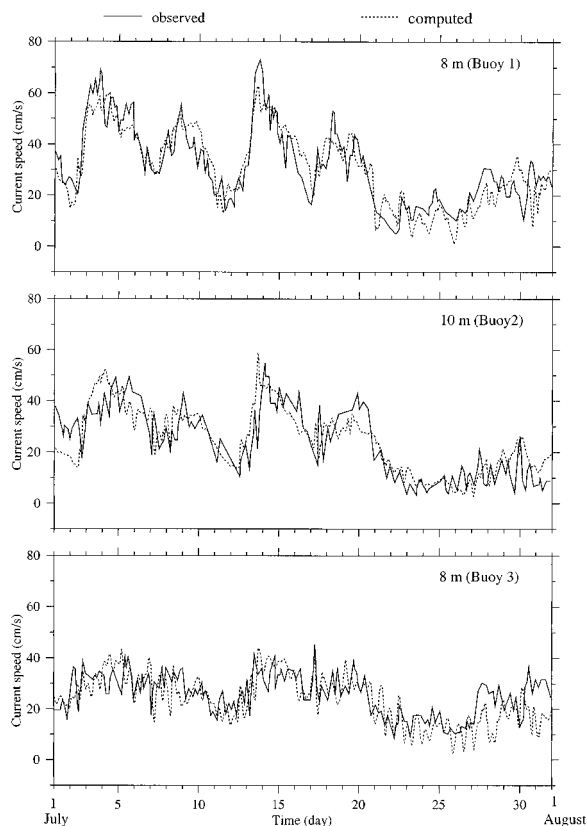


FIG. 10. Comparisons of model-predicted and observed current speed at a depth of 8–10 m at Buoys 1, 2, and 3. Solid line: observed; dashed line: model predicted.

significantly during southward, southwestward, or southeastward winds. For example, on the second model day after the wind forcing was applied, the relatively strong northeastward wind (with a speed of $8\text{--}9\text{ m s}^{-1}$) advected water onshore, and thus dramatically increased the eastward alongshelf and downwelling flows along the Keweenaw coast (Figs. 8a and 9a). The alongshelf current accelerated 40 cm s^{-1} over one day. This maximum speed of 60 cm s^{-1} occurred during the same period as the maximum northeastward wind and was located near the coast (Fig. 10, upper panel). The strong downwelling flow caused a relatively strong vertical mixing near the coast, which led to a relatively large, cross-shelf temperature gradient throughout the water column. The alongshelf current jet, which had been restricted to the upper 25 m, extended to the bottom at the coast (Fig. 9a). Vertical velocity on the slope was about 0.005 cm s^{-1} .

The eastward alongshelf current continued to penetrate deeper during northeastward downwelling-favorable winds. On the fifth model day, the water column was vertically well mixed, and the eastward alongshelf current was present throughout the entire 250-m water column over the slope (Figs. 8b and 9b). The model also predicted two cyclonic, cross-shelf, secondary cir-

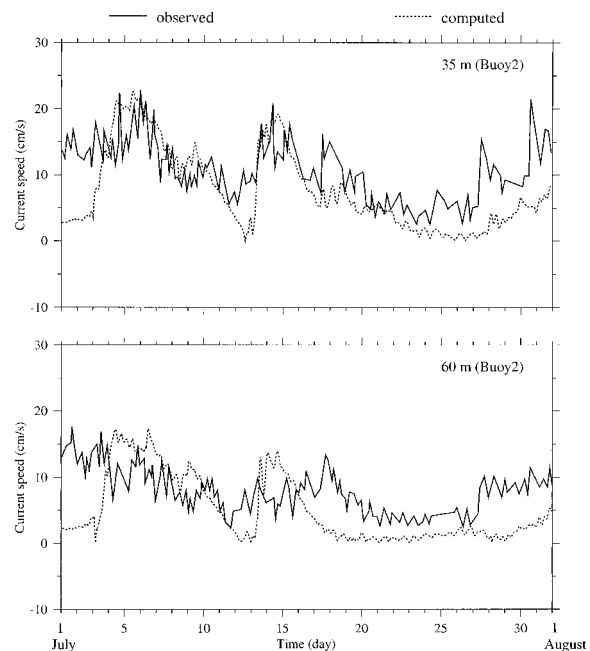


FIG. 11. Comparisons of model-predicted and observed current speed at depths of 35 and 60 m at Buoy 2. Solid line: observed; dashed line: model predicted.

ulation cells within 5 km of the coast, with a downwelling velocity of about 0.004 cm s^{-1} and an upwelling velocity of about 0.005 cm s^{-1} (Fig. 9b).

The southwestward wind, which prevailed during the 9th and 11th model days (after the wind forcing was applied), produced an upwelling along the slope and thus an offshore Ekman transport near the surface. As a result, the alongshelf jet current significantly subsided near the coast, and a reversed current was found offshore (Fig. 8c). The maximum speed of the current, which was about $40\text{--}60\text{ cm s}^{-1}$ during the downwelling events, dropped to 20 cm s^{-1} (Figs. 9c and 10a). Upwelling moved the cold water upslope, which caused an upward compression of temperature contours and hence led to a surface-intensified jet near the coast (Fig. 9c). The offshore Ekman transport also tended to advect the thermal front offshore, and thus caused an offshore shift of the alongshelf jet current. A similar response of currents to wind was found on the 15th model day when a cyclonic-rotating, southwestward wind prevailed (Figs. 8d and 9d).

The model-predicted speed of the jet was in good agreement with current meter data taken at buoys 1, 2, and 3 near Eagle Harbor (Figs. 10 and 11). Based on the observation, the speed of the Keweenaw Current near the surface varied with the wind over a period of 5 days. Four peaks occurred in the current meter records in early and middle July during the northeastward downwelling-favorable wind events. The observed Keweenaw Current decreased rapidly offshore and with depth. For example, on 4 July, the observed maximum speed

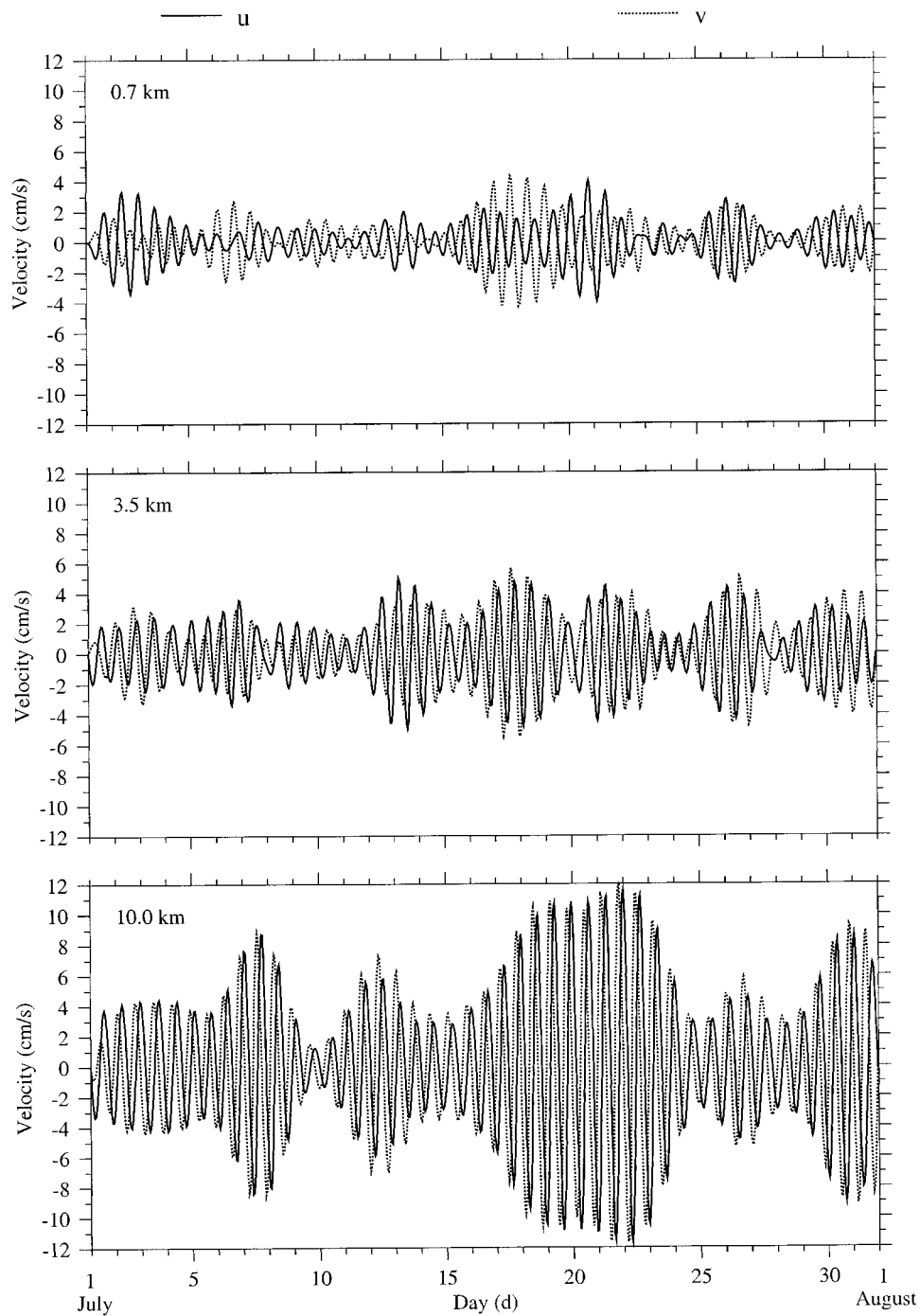


FIG. 12. Time series of the band-pass filtered surface near-inertial velocity components (u : alongshelf and v : cross-shelf) at locations that were 0.7, 2.5, and 10 km away from the coast, respectively. Solid line: u and dashed line: v . The frequency band used in the filtering was $1/14$ h to $1/19$ h. The local inertial frequency is $1/16.4$ h.

near the surface was about 70 cm s^{-1} at buoy 1; however, it decreased to 50 cm s^{-1} at buoy 2 and 38 cm s^{-1} at buoy 3, over a distance of about 1.8 km (buoys 1 and 2) or 2.8 km (buoys 1 and 3), respectively. At the same time, the speed of the current decreased about 20 cm

s^{-1} at a depth of 35 m at buoy 2, 30 cm s^{-1} slower than that measured at a depth of 10 m. All of these structures were reproduced in the model simulation.

On the other hand, we did not expect that our model result would exactly match with observations. After 14

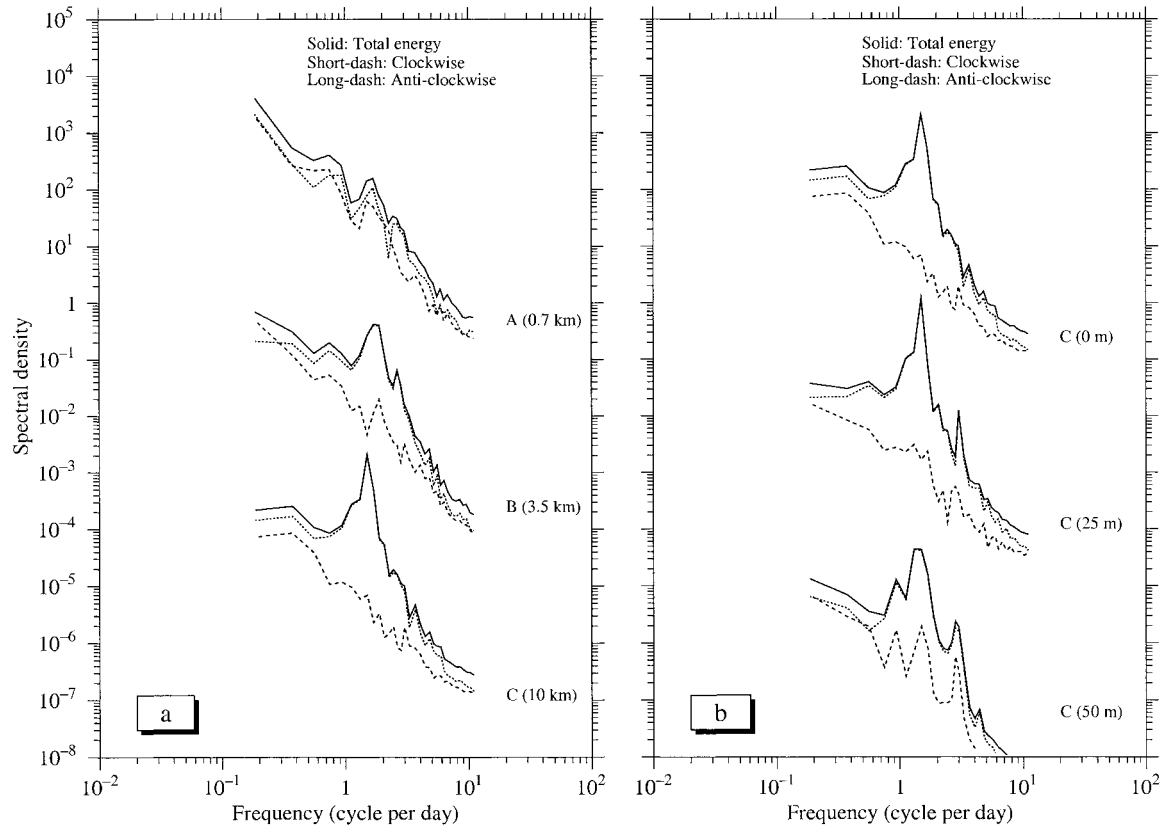


FIG. 13. Rotary spectra of the model-predicted current at 8–10 m at (a) stations A, B, C and at depths of 10, 25, and 50 m at station C. The spectra at 25 and 50 m are shifted downward by 10^4 . Estimates of rotary spectra were made using the hourly current data from 1 to 31 Jul 1973. Segments of 128 points with an overlap of 64 points were used for spectrum analysis. Spectrum density is in $(\text{cm s}^{-1})^2 \text{cpd}^{-1}$.

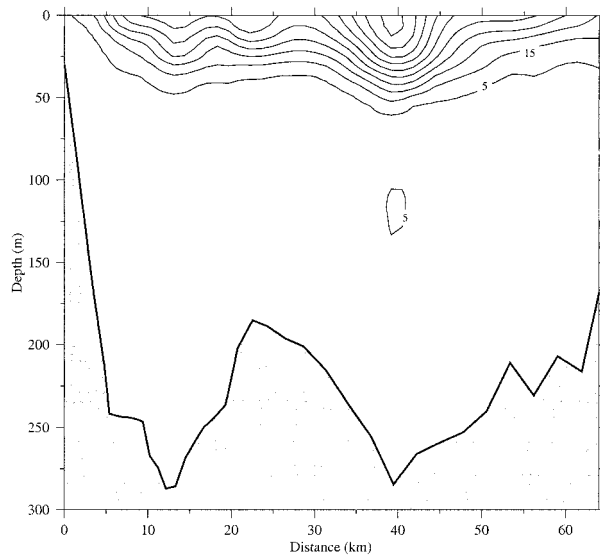


FIG. 14. Cross-shelf distribution of the model-predicted bandpassed near-inertial current variance from 1 to 31 Jul 1973 on section 1 (see Fig. 1 for location). The contour units are $\text{cm}^2 \text{s}^{-2}$.

July, the wind rotated significantly, which generated the significant near-inertial oscillations. A big difference between model-predicted and observed currents in the deep region was probably caused by a downward energy propagation of near-inertial internal waves associated with the temporal variation of wind and heat flux. This question, however, could not be addressed in the present modeling experiments because no hourly sampled heat flux data were available during that period.

b. Near-inertial oscillations

Relatively strong near-inertial oscillations occurred episodically in the model simulation for July 1973 (Fig. 12). These oscillations were weak near the coast and increased significantly offshore. The oscillating currents were characterized by an ellipse near the coast due to the restriction of no water flux at the coastal boundary and interaction with the coastal jet. The currents became more circular on the offshore side of the jet and in the interior. These oscillations usually occurred during an anticyclonic-rotating wind event with a timescale of 5 days. The maximum amplitude of the oscillations at the center of the lake reached 15 cm s^{-1} , occurring about

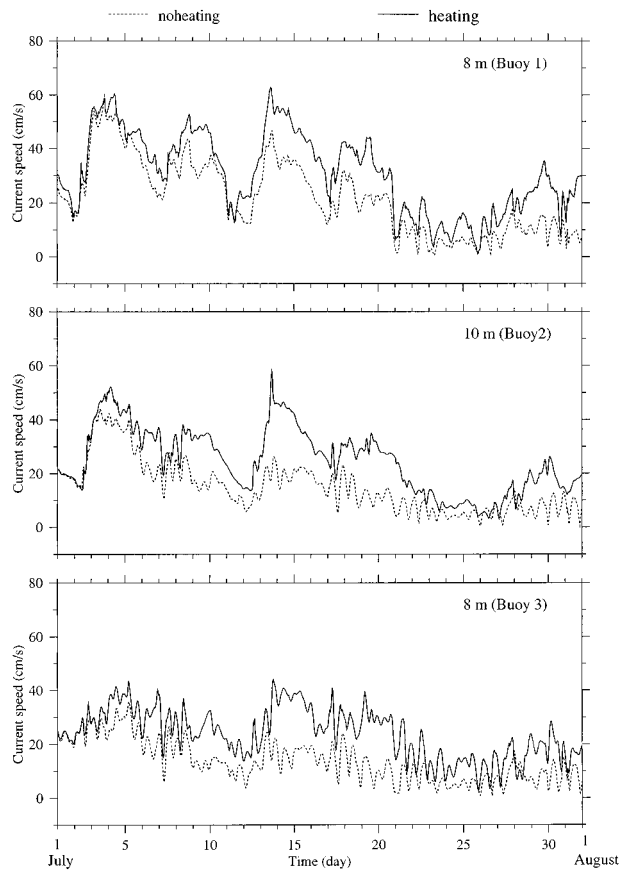


FIG. 15. Time series of the model-predicted current speeds at 8–10 m at Buoys 1, 2, and 3 for the cases with (solid line) and without (dashed line) heating for Jul 1973.

20 July when the wind suddenly rotated anticyclonically.

The maximum energy was found for oscillations with a period of 18 h near the coast, and this period was reduced to 16 h offshore, 1.6 higher and 0.4 lower than the local inertial period, respectively (Fig. 13). The energy of the near-inertial oscillations was restricted to the upper 50 m. It was most intense at the surface and decreased rapidly with depth and was at its maximum in the lake's interior (Fig. 14). These near-inertial oscillations dominated short-term variations in the lake during the summer of 1973. The temporal and spatial variations of the near-inertial oscillations were very similar to those in Lake Ontario found by Marmorino (1978), and the physical mechanism responsible for the occurrence of these inertial oscillations was the same as those found over the Texas and Louisiana shelf by Chen et al. (1996) and Chen and Xie (1997). The near-inertial spectral peak shift from the local inertial frequency as a function of cross-shelf position can be easily interpreted using the theory of inertial–internal waves in a jet proposed by Mooers (1975). This theory suggests that the anticyclonic and cyclonic shears (relative vorticity) of a current jet can cause a frequency shift of the cross-stream propa-

gation of inertial–internal waves. (The animation of the model simulation and near-inertial oscillation can be viewed at <http://whale3.marsci.uga.edu>.)

4. Physical mechanisms

The good agreement between model-predicted and observed currents at three buoys suggests that the model has captured the physical processes that controlled the temporal and spatial variations of the Keweenaw Current near the surface. The model results showed that the temporal variation of the current was dominantly driven by windforcing. The alongshelf current intensified during the northeastward downwelling-favorable wind event and weakened during the southwestward or northwestward upwelling-favorable wind event.

What is the role of surface heating in this dynamic system? To address this question, the model was run excluding heat forcing. The model results indicated that ignoring heat flux led to underestimates of the current peaks that occurred during the downwelling-favorable wind events in early and middle July (Fig. 15). This result suggests that heating played a key role in maintaining the intensity of the thermal bar, and thus indirectly contributed to the intensification of the Keweenaw Current during downwelling-favorable wind events in the summer. A successful simulation of the Keweenaw Current with the observed synoptic wind and monthly averaged surface heat flux, on the other hand, implied that short-term temporal variation in surface heating had little influence on the low-frequency variation of the Keweenaw Current during the summer.

As an alternative analysis, the momentum balance for downwelling- and upwelling-favorable events was examined. From 11 to 13 July, for example, in the case with heating, the strong northeastward (downwelling favorable) wind advected the water onshore near the surface and increased the cross-shelf gradient of surface elevation, leading to an acceleration of the alongshelf current (Fig. 10). In the cross-shelf momentum equation, the alongshelf current was geostrophic, with a basic balance between the Coriolis force and cross-shelf gradient forces of surface elevation and density (Fig. 16, lower panel). This current decreased dramatically with depth due to the downward increase of the cross-shelf baroclinic pressure gradient. In the alongshelf momentum equation, the local change of the alongshelf current was mainly controlled by vertical diffusion (linked with the wind stress) and an alongshelf gradient of surface elevation (Fig. 16, upper panel). The current decreased with depth due to the downward decrease of the vertical diffusion. In the case without heating, the alongshelf current was still geostrophic but it was mainly dominated by a barotropic process with a basic balance between Coriolis force and cross-shelf gradient of surface elevation (Fig. 16, lower panel). Near the surface, the local change of the alongshelf current was mainly controlled by vertical diffusion, horizontal advection, and Coriolis deflection

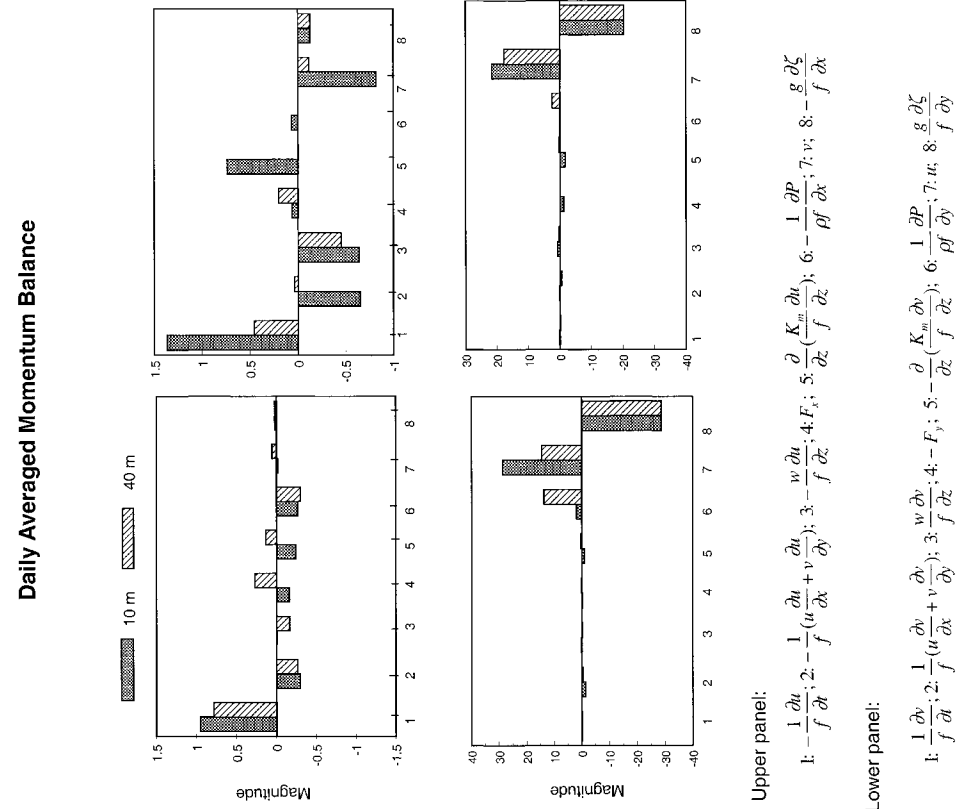


FIG. 16. Daily averaged terms in the momentum equations for a downwelling event during 11.5-12.5 Jul 1973 for the cases with (left) and without (right) heating.

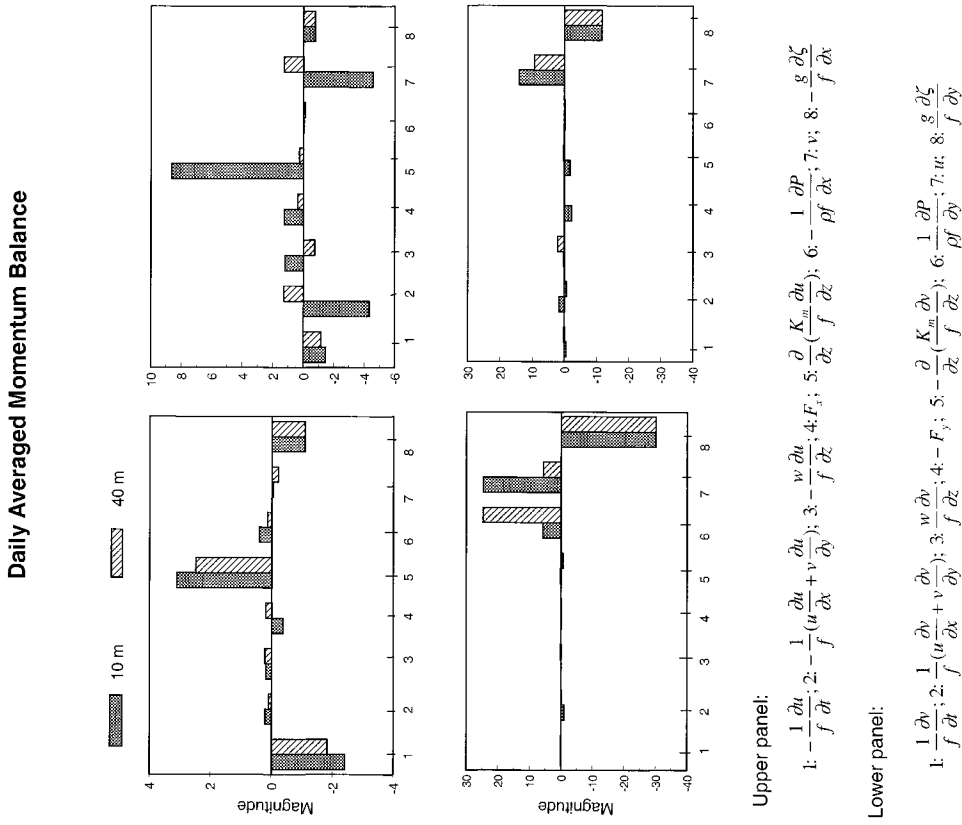


FIG. 17. Daily averaged terms in the momentum equations for an upwelling event during 14.5-15.5 Jul 1973 for the cases with (left) and without (right) heating.

(Fig. 16, upper panel). As the vertical diffusion rapidly decreased with depth, vertical advection and the along-shelf gradient of surface elevation became important in the along-shelf momentum balance.

In an upwelling event that occurred during 14–16 July, the alongshelf current was again geostrophic. It decreased significantly with depth in the case with heating but was dominated by a barotropic mode in the case without heating (Fig. 17, lower panel). Unlike the downwelling-favorable event, in cases both with and without heating, the local change of the alongshelf current was controlled mainly by a more complex nonlinear process associated with horizontal and vertical advection, along-shelf pressure forcing, and horizontal and vertical diffusions (Fig. 17, upper panel).

Comparison of the momentum balance between the cases with and without heating suggested that heating played a key role in maintaining the thermal structure along the Keweenaw coast and hence indirectly contributed to the intensification of the alongshelf current in summer. The cross-shelf baroclinic pressure gradient, which is determined by the cross-shelf temperature gradient across the thermal front, was a key forcing that balanced the vertical shear of the alongshelf current and hence led to the large cross-shelf water transport during the downwelling-favorable wind event. This large onshore water transport significantly increased the cross-shelf surface pressure gradient, and thus intensified the alongshelf current.

The dominant physical processes during the upwelling-favorable and downwelling-favorable wind events were very different. Although the momentum balance in the cross-shelf direction remained the same in these two cases, the alongshelf momentum balance was more complex during the upwelling-favorable wind event. Near the surface, almost all terms, such as the horizontal advection, alongshelf density gradient, horizontal diffusion, and vertical diffusion made similar contributions to the local change of the alongshelf current. The vertical advection associated with upwelling became significant with depth.

5. Conclusions

The Keweenaw Current, as observed along coast of the Keweenaw Peninsula in Lake Superior during July 1973, was simulated using a 3D, nonorthogonal coordinate transformation, primitive equation model. The model results have shown that the structure of the thermal bar and coastal jet current varied significantly with wind. The eastward alongshelf current tended to intensify dramatically during a northward or northeastward wind and to subside significantly during a southward or southwestward or southeastward wind. The model-predicted alongshelf current near the surface was in good agreement with observed currents at buoy stations near Eagle Harbor. A poor model–data comparison in the deep region was probably due to the lack of the physical

mechanism for a downward energy propagation of near-inertial internal waves associated with the short-term variation of surface heat flux.

The numerical experiments revealed that heating played a critical role in maintaining the intensity of the thermal bar, and, hence, indirectly contributed to the intensification of the alongshelf current during the summer. The cross-shelf baroclinic pressure gradient (determined by the cross-shelf temperature gradient across the thermal front) was the key forcing that balanced the vertical shear of the alongshelf current and hence led to the large cross-shelf water transport during the downwelling-favorable wind event. This large onshore water transport significantly increased the cross-shelf surface pressure gradient, and thus intensified the alongshelf current.

Relatively strong near-inertial oscillations were observed episodically in the model simulations for July 1973. These oscillations were intensified at the surface, weak near the coast and became significantly stronger offshore. The frequency of the oscillations at the energy peak was lower than the local inertial frequency near the coast, but it was higher offshore, consistent with the effects of the baroclinic mean flow (i.e., due to the anticyclonic and cyclonic shear zone of the Keweenaw Current jet) on the effective inertial frequency (Moore 1975). These oscillations were usually associated with the anticyclonic-rotating wind events with a timescale of 5 days. The maximum amplitude of the oscillations, which reached 15 cm s^{-1} at the center of the lake, occurred during a sudden change in the wind direction.

Acknowledgments. This research was supported by the National Science Foundation under Grants OCE-9712869 for Changsheng Chen, OCE-9712871 for Elise Ralph, and OCE-9712872 for Sarah Green. We thank Joe Niebauer for the figures of observed currents taken near Eagle Harbor in July 1973 and for his constructive comments and suggestions. We also thank George Davidson for his editorial help with this manuscript. Two anonymous reviewers have provided many constructive suggestions and their help is greatly appreciated.

REFERENCES

- Bennett, E. B., 1978: Characteristics of the thermal regime of Lake Superior. *J. Great Lakes Res.*, **4** (3–4), 310–319.
- Blumberg, A. F., and G. L. Mellor, 1987: A description of a three-dimensional coastal ocean circulation model. *Three-Dimensional Coastal Models*, N. Heaps, Ed., Coastal and Estuarine Sciences Ser., Vol. 5, Amer. Geophys. Union, 1–16.
- Chen, C., and L. Xie, 1997: A numerical study of wind-induced, near-inertial oscillations over the Texas–Louisiana Shelf. *J. Geophys. Res.*, **102** (C2), 15 583–15 593.
- , R. O. Reid, and W. D. Nowlin, Jr., 1996: Near-inertial oscillations over Texas–Louisiana Shelf. *J. Geophys. Res.*, **101** (C2), 3509–3524.
- , L. Zheng, and J. Zhu, 2000: A nonorthonormal coordinate coastal circulation model. *J. Atmos. Oceanic Technol.*, submitted.
- , J. Zhu, E. Ralph, S. A. Green, J. Wells Budd, and F. Y. Zhang, 2001: Prognostic modeling studies of the Keweenaw Current in

- Lake Superior. Part I: Formation and evolution. *J. Phys. Oceanogr.*, **31**, 379–395.
- Diehl, S., W. Maanum, T. Jordan, and M. Syldor, 1977: Transports in Lake Superior. *J. Geophys. Res.*, **82**, 977–978.
- Harrington, M. W., 1895: Surface current of the Great Lakes. *Weather Bureau Bulletin*, U.S. Department of Agriculture.
- Kraus, E. B., 1972: *Atmosphere–Ocean Interaction*. Clarendon Press, 275 pp.
- Lam, D. C., 1978: Simulation of water circulation and chloride transports in Lake Superior for summer 1973. *J. Great Lakes Res.*, **4**, 343–349.
- Large, W. S., and S. Pond, 1981: Open ocean momentum flux measurements in moderate to strong winds. *J. Phys. Oceanogr.*, **11**, 1076–1084.
- Marmorino, G. O., 1978: Inertial currents in Lake Ontario, winter 1972–73 (IFYGL). *J. Phys. Oceanogr.*, **8**, 1104–1120.
- Mellor, G. L., and T. Yamada, 1982: Development of a turbulence closure model for geophysical fluid problem. *Rev. Geophys. Space Phys.*, **20**, 851–875.
- Mooers, C. N. K., 1975: Several effects of a baroclinic current on the cross-stream propagation of inertial-internal waves. *Geophys. Fluid Dyn.*, **6**, 245–275.
- Niebauer, H. J., T. Green, and R. A. Ragotzkie, 1977: Coastal upwelling/downwelling cycles in southern Lake Superior. *J. Phys. Oceanogr.*, **7**, 918–927.
- Schertzer, W. M., 1978: Energy budget and monthly evaporation estimates for Lake Superior, 1973. *J. Great Lake Res.*, **4**(3–4), 320–330.
- Simpson, J. J., and T. D. Dickey, 1981a: The relationship between downward irradiance and upper ocean structure. *J. Phys. Oceanogr.*, **11**, 309–323.
- , and —, 1981b: Alternative parameterizations of downward irradiance and their dynamical significance. *J. Phys. Oceanogr.*, **11**, 876–882.